Inorganic Chemistry

Article

pubs.acs.org/IC

EPR, Resonance Raman, and DFT Calculations on Thiolate- and Imidazole-Bound Iron(III) Porphyrin Complexes: Role of the Axial Ligand in Tuning the Electronic Structure

Pradip Kumar Das, Sudipta Chatterjee, Subhra Samanta, and Abhishek Dey*

Department of Inorganic Chemistry, Indian Association for the Cultivation of Science, Kolkata, India 700032

Supporting Information

ABSTRACT: Iron(III) porphyrin complexes bearing covalently attached imidazole and thiolate axial ligands are investigated using resonance Raman, electron paramagnetic resonance, and cyclic voltammetry. The thiolate ligand stabilizes a low-spin ground state in solvent-bound six-coordinate species, weakens the Fe−N_{pyr} bonds, and shifts the $Fe^{III/II}$ potential more negative by ∼500 mV relative to an imidazole-bound species. Density functional theory calculations reproduce the experimental observation and indicate that the covalent charge donation from thiolate to iron reduces the Z_{eff} on the iron. This increases the Fe_{3d} orbital energies, which changes the bonding interaction present in these complexes significantly. In particular, the increase of the Fe_{3d} energies activates an iron-to-porphyrin π^*-back-bonding interaction not present in the imidazole-bound complex.

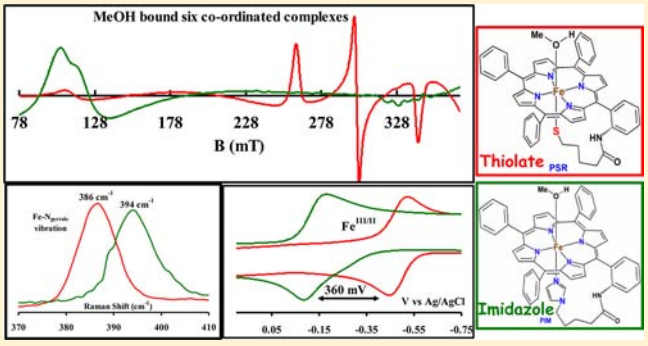

INTRODUCTION

Thiolate-bound iron porphyrin cofactors are found in several metalloenzymes, e.g., cytochrome P450 (cyt P450), NO synthase, and chloroperoxidase.[1−6] Out of these, cyt P450 has been of particular interest to the catalysis community because of its capability of oxidizing inert C−H bonds using molecular O_2.[2] The remarkable reactivity of this heme enzyme is mostly attributed to the presence of the proximal thiolate ligand in the active site, which is proposed to exert a "push effect".[7−13] The Fe center in the active site of cyt P450 in its resting form (Figure 1) is best described as a six-coordinate (6C), low-spin (LS; $S = {}^1/_2$) Fe^{III}.[14,15] Upon substrate binding, a five-coordinate (5C), high-spin (HS; $S = {}^5/_2$) Fe^{III} site is formed and is reduced to generate a HS ($S = 2$) Fe^{II} active form that binds O_2.[16−18] The "push effect" of the thiolate ligand has been proposed to lower the $Fe^{III/II}$ reduction potential, weaken the axial ligand binding, and affect the heterolytic O−O bond cleavage of a Fe^{III}-OOH species (compound 0)[4] without requiring an acidic proton to drive it, resulting in the formation of a highly oxidizing species known as compound I.[8,16−25] Several investigations, both theoretical and experimental, have focused on the nature of the "push effect", and both electrostatic (thiolate is an anionic ligand) and orbital overlap (Fe−S bonds are very covalent) have been invoked to play roles.[13,14,17,26−32] However, it is difficult to quantitatively evaluate these effects in the protein active site because of the possible involvement of second-sphere interactions, e.g., hydrogen bonding, steric, etc.[33,34] Rather, well-defined synthetic models offer a simpler platform to investigate these effects.

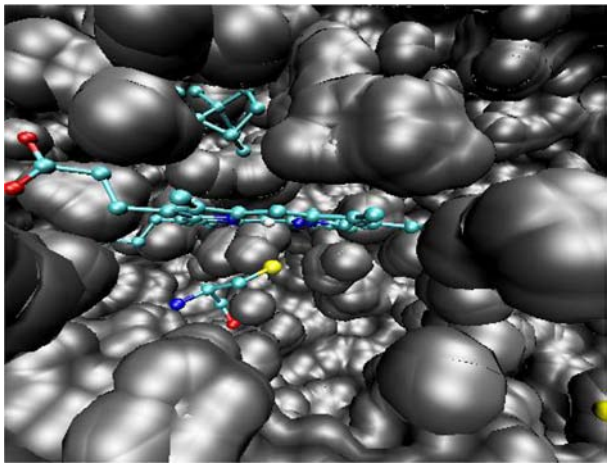

Figure 1. Active site structure of a cyt P450 enzyme (pdb id: 1AKD).

The synthesis of a thiolate-bound iron(III) porphyrin complex is complicated by the $2Fe^{III} + RS \rightleftarrows 2Fe^{II} + RS{-}SR$ equilibrium. So far, few synthetic models of an oxidized cyt P450 active site are reported that mimic the axial thiolate coordination to an iron(III) porphyrin.[35−41] Some models bear aromatic thiolate ligands and are HS in a noncoordinating solvent like CH_2Cl_2.[42−44] On the contrary, the aliphatic/benzylic thiolate-coordinated models offer a 6C LS complex

Received: May 14, 2012
Published: September 26, 2012

dx.doi.org/10.1021/ic3016035 | Inorg. Chem. 2012, 51, 10704−10714

with a solvent molecule bound to the iron as the sixth ligand.[45] Some of these models are known to hydroxylate C−H bonds of intermediate strength using peracids/peroxides.[42] Most of these synthetic models are extremely unstable under O_2 even in their oxidized ferric state.[44,46] Previous studies demonstrated that the nature of the Fe−S bond in the cyt P450 active site and related synthetic model complexes is much more covalent relative to that of a neutral ligand.[43]

Thiolate is a weak-field ligand because it can act as σ and π donors. Imidazole (most abundant heme-coordinating residue in nature), on the other hand, is a strong-field ligand because it mainly acts as a strong σ donor. However, many water (H_2O)-bound histidine (imidazole headgroup)-coordinated ferric heme sites are, in fact, HS, whereas the H_2O-bound cysteine (thiolate headgroup)-coordinated ferric heme sites are LS, which is counterintuitive.[47] The same is true for synthetic model complexes; i.e., imidazole-coordinated H_2O/solvent-bound complexes are HS, whereas thiolate-coordinated H_2O/solvent complexes are LS. This, however, is not the case for nonheme systems.[48] The 6C active site of superoxide reductase (SOR), which bears an axial cysteine ligand, is HS in both resting and several ligand-bound states.[49] This implies the presence of an unusual bonding phenomenon in thiolate-ligated heme complexes that needs to be understood.

In our pursuit of a synthetic analogue of cyt P450, we have been able to synthesize two thiolate-bound iron(III) porphyrin complexes in which the porphyrin macrocycle and thiolate functional group are held by a flexible linker (PSR or PPSR; Figure 2). One of the 5C molecules (PPSR; Figure 2) has the thiolate arm sterically protected in a hydrophobic environment, and the other has the thiolate arm exposed (PSR; Figure 2). To understand the effect of thiolate on the properties of the Fe center, an analogous complex is synthesized in which the same linker bears an imidazole headgroup (PIM; Figure 2) instead of a thiolate.[50−52] In this study, we use electron paramagnetic resonance (EPR), resonance Raman (rR), cyclic voltammetry (CV), and density functional theory (DFT) calculations to investigate the electronic structure of these complexes.

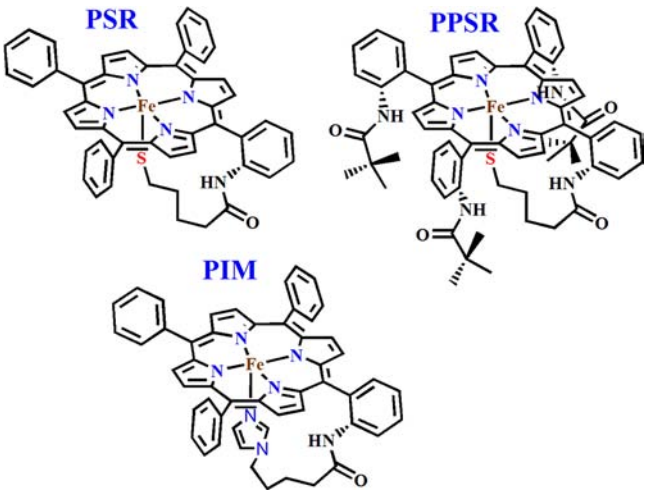

Figure 2. Schematic diagrams of the PSR, PPSR, and PIM complexes.

EXPERIMENTAL DETAILS

Materials. Benzaldehyde (99%), 2-nitrobenzaldehyde (98%), pyrrole (98%), 5-bromovaleroyl chloride (97%), 5-chlorovaleroyl chloride (96%), potassium thioacetate (98%), ferrous bromide (98%), 2,4,6-collidine (99%), and chloroform-*d* (99.8%) were purchased from Aldrich Chemical Company. Tetrahydrofuran (THF), acetonitrile (CH_3CN), dimethylformamide (DMF), dichloromethane (DCM), methanol (MeOH), diethyl ether, acetic acid, stannous chloride ($SnCl_2{\cdot}2H_2O$), and anhydrous Na_2SO_4 were purchased from Merck. All solvents were purified by standard procedures. Pyrrole and 2,4,6-collidine were distilled directly before use. *meso*-Mono(*o*-aminophenyl)triphenylporphyrin[50] and *meso*-tetra(*α,α,α,α-o*-aminophenyl)porphyrin (TAPP)[37] were synthesized using reported methods. Insertion of the iron into porphyrins followed known routes.[37] Column chromatography was done on 60−120 mesh silica gel, purchased from SRL. Thin-layer chromatography (TLC) was done on commercially prepared silica gel or alumina plates purchased from Merck.

Instrumentation. UV−vis absorption data were obtained from an Agilent Technologies model 8453 spectrophotometer fitted with a diode-array detector. All of the ^{1}H NMR spectra were recorded on a Bruker DPX-300 or DPX-500 spectrometer at room temperature. The EPR spectra were recorded on a JEOL instrument. The mass spectra were recorded by a QTOF Micro YA263 instrument. All electrochemical experiments were performed using a CH Instruments model CHI710D electrochemical analyzer. rR data were collected using a 413.1 nm excitation wavelength from a Kr^+ ion source (Coherent, Sabre Innova SBRC-DBW-K) and a Trivista 555 triple spectrophotometer (gratings used in the three stages were 900, 900, and 1800 grooves/mm) fitted with a Pixis CCD camera (Princeton Instruments). The optics (e.g., plano−convex lenses, mirrors, etc.) for collection of the rR data were purchased from Sigma-koki, Japan.

Electrochemical Measurements. The CV experiments were performed on CH Instruments bipotentiostat models 700D and 610D. A glassy carbon electrode was used as the working electrode. A platinum wire was used as the counter electrode. The measurements were made against an Ag/AgCl reference electrode with scan rates varying from 50 to 500 mV. The solutions were comprised of 1 mM complex and 100 mM tetrabutylammonium perchlorate (TBAP) as the supporting electrolyte.

Synthesis and Characterization. The synthetic strategy is described in detail in Scheme 1.

*1. meso-Mono(o-5-bromovaleramidophenyl)triphenylporphyrin (**1**).* 5-Bromovaleroyl chloride (26 μL, 1.2 equiv) was dissolved in 5 mL of dry THF, added dropwise over a period of 30 min to a solution of *meso*-mono(*o*-aminophenyl)triphenylporphyrin[50] (100 mg, 0.158 mmol) in 20 mL of dry THF, and cooled to 0 °C. When the addition was complete, the resulting solution turned green. Aqueous ammonia was added dropwise until the solution became purple. The solution was then poured into a separating funnel. A total 50 mL of CH_2Cl_2 was added and washed with 2 × 30 mL of 10% $NaHCO_3$ and 2 × 30 mL of H_2O. The organic layer was collected and dried over anhydrous Na_2SO_4. The solvent was then evaporated on a rotary evaporator, and the residue was purified by chromatography on a column packed with 60−120 mesh silica gel in hexane using 80% DCM/hexane mixture as the eluent. Yield: 119.62 mg (∼95%).

Anal. Calcd for $C_{49}H_{38}BrN_5O$: C, 74.24; H, 4.83; N, 8.83. Found: C, 73.34; H, 4.95, N, 8.72. ^{1}H NMR ($CDCl_3$): δ −2.72 (s, 2H), 1.07 (m, 2H), 1.19 (m, 2H), 1.34 (m, 2H), 2.75 (t, 2H, J = 6.6 and 6.3 Hz), 6.74 (s, 1H), 7.54 (t, 1H, J = 7.2 and 7.5 Hz), 7.83 (m, 10H), 8.06 (d, 1H, J = 7.5 Hz), 8.23 (m, 6H), 8.72 (d, 1H, J = 8.4 Hz), 8.78 (d, 2H, J = 4.8 Hz), 8.89 (s, 6H). ESI-MS (positive-ion mode, MeOH): m/z 792.34 (90%; $[M]^+$).

*2. meso-Mono(o-5-thioacetatovaleramidophenyl)-triphenylporphyrin (**2**).* Potassium thioacetate (17.2 mg, 1.2 equiv) was added to the solution of **1** (100 mg, 0.126 mmol) taken in 25 mL of dry and degassed DMF, and the reaction was refluxed for 8 h in the dark under N_2 atmosphere. The formation of the desired product was monitored by TLC. After quenching the reaction mixture with H_2O, diethyl ether was added to collect the product in the organic layer. Then it was dried over anhydrous Na_2SO_4. After removal of the solvent, the product was purified by column chromatography using a 1% MeOH/DCM mixture as the eluent. Yield: 92.44 mg (∼93%).

dx.doi.org/10.1021/ic3016035 | *Inorg. Chem.* 2012, 51, 10704−10714

Scheme 1. General Synthetic Procedure

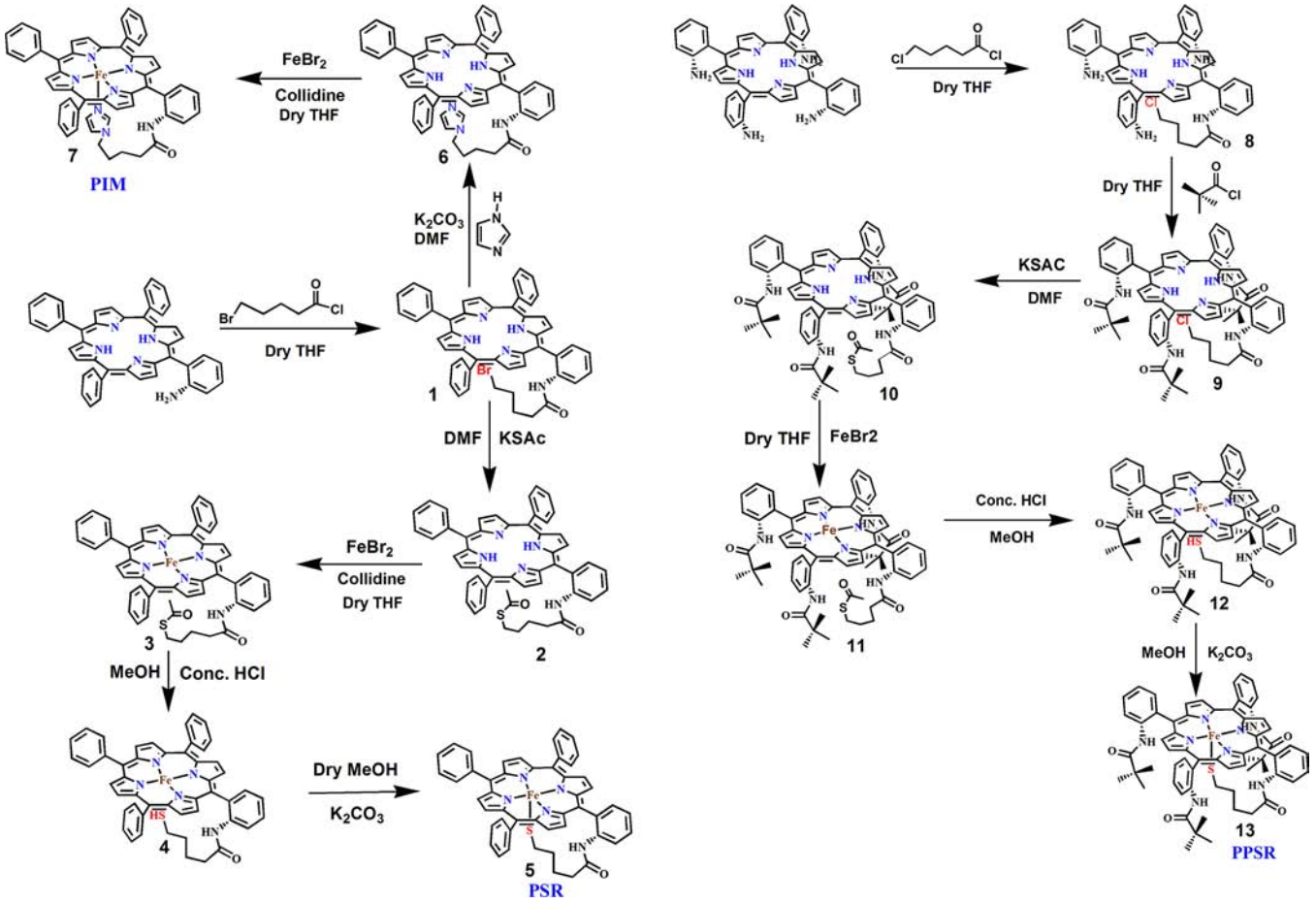

Anal. Calcd for $C_{51}H_{41}N_5O_2S$: C, 77.74; H, 5.24; N, 8.89. Found: C, 76.78; H, 5.62; N, 8.69. ^{1}H NMR ($CDCl_3$): δ −2.72 (s, 2H), 0.86−0.96 (m, 4H), 1.35 (m, 2H), 1.872 (s, 3H), 2.2 (t, 2H, J = 4.2 Hz), 6.77 (s, 1H), 7.52 (t, 1H, J = 4.2 and 4.5 Hz), 7.69−7.89 (m, 10H), 8.04 (d, 1H, J = 4.2 Hz), 8.18−8.24 (m, 6H), 8.71 (d, 1H, J = 4.8 Hz), 8.78 (d, 2H, J = 2.7 Hz), 8.89 (s, 6H). ESI-MS (positive-ion mode, CH_3CN): m/z 788.35 (100%; $[MH]^+$).

UV−vis (THF): λ_{max}/nm = 418, 515, 550, 595, 650.

*3. meso-Mono(o-5-thioacetatovaleramidophenyl)-triphenylporphyrinatoiron(III) Bromide (**3**).* Thioacetate-functionalized porphyrin **2** (100 mg, 0.126 mmol) was dissolved in 15 mL of dry and degassed THF. 2,4,6-Collidine (34 μL, 2 equiv) was added to this solution followed by the addition of $FeBr_2$ (109 mg, 4 equiv). The solution was stirred overnight in a glovebox in the dark. The reaction mixture was quenched by H_2O followed by the addition of DCM. The organic layer was washed with a brine solution and was collected and dried over anhydrous Na_2SO_4. The solvent was removed on a rotary evaporator, and the residue was separated by chromatography on a column packed with 60−120 mesh silica gel in CH_2Cl_2. The column was eluted with a 4% MeOH/CH_2Cl_2 mixture. Yield: 98 mg (∼92%).

Anal. Calcd for $C_{51}H_{39}BrFeN_5O_2S$: C, 66.46; H, 4.26; N, 7.60. Found: C, 66.06; H, 4.52; N, 7.12. ESI-MS (positive-ion mode, CH_3CN): m/z 841.24 (100%; $[M]^+$).

UV−vis (THF): λ_{max}/nm = 345, 414, 508, 576.

*4. meso-Mono(o-5-thiolvaleramidophenyl)-triphenylporphyrinatoiron(III) Bromide (**4**).* Thioacetate-functionalized iron porphyrin **3** (100 mg, 0.118 mmol) was taken in 15 mL of a degassed mixture of concentrated HCl and MeOH (1:14). The solution was then refluxed under N_2 atmosphere in the dark. The reaction mixture was worked up with H_2O and DCM. The organic layer was washed with a brine solution. It was dried over anhydrous Na_2SO_4 and was purified by column chromatography using a 95:5 dry DCM/MeOH mixture in a N_2 atmosphere. Yield: 86 mg (∼90%).

Anal. Calcd for $C_{49}H_{37}BrFeN_5OS$: C, 66.90; H, 4.24; N, 7.96. Found: C, 65.84; H, 4.90; N, 7.26. ESI-MS (positive-ion mode, CH_3CN): m/z 799.06 (10%; $[M]^+$), 840.98 (25%; $[M]^+$ + CH_3CN), 683 (100%; $[M]^+$ − tail linker).

UV−vis (THF): λ_{max}/nm = 372, 418, 508, 579.

*5. meso-Mono(o-5-thiolatevaleramidophenyl)-triphenylporphyrinatoiron (PSR; **5**).* Thiol-functionalized porphyrin **4** (86 mg, 0.107 mmol) was dissolved in 15 mL of dry and degassed MeOH in the presence of activated K_2CO_3. The solution was stirred overnight in a glovebox. The reaction mixture was then filtered using Whatmann 40, and the filtrate was evaporated and dried using a vacuum pump inside the glovebox. Yield: 77 mg (∼90%).

UV−vis (THF): λ_{max}/nm = 332, 414, 574.

*6. meso-Mono[o-5-(N-imidazolyl)valeramidophenyl]-triphenylporphyrin (**6**).* Collman et al. first reported an imidazole tail porphyrin.[50] Here we synthesized PIM by a different approach. **1** (100 mg, 0.125 mmol) was dissolved in 10 mL of degassed DMF under N_2 atmosphere. A solution of 18 mg of imidazole in 2 mL of DMF was added in the presence of K_2CO_3, and the resulting solution was allowed to reflux under a N_2 atmosphere in the dark for 8 h. The solution was then poured into 100 mL of diethyl ether, washed with 100 mL of H_2O, and dried over anhydrous Na_2SO_4. The solvent was evaporated on a rotary evaporator and the residue separated by flash chromatography (5% MeOH in CH_2Cl_2). Yield: 90 mg (90%).

Anal. Calcd for $C_{52}H_{41}N_7O$: C, 80.08; H, 5.30; N, 12.57. Found: C, 77.94; H, 5.95, N, 10.72. ^{1}H NMR ($CDCl_3$): δ −2.64 (s, 2H), 0.2−3 [8H, −$(CH_2)_4$−], 7.7−7.79 (m, 15H), 7.8 (5H), 8.83 (3H), 8.79 (1H), 8.9 (7H), 8.96 (1H). ESI-MS (positive-ion mode, MeOH): m/z 780 (20%; $[M]^+$).

UV−vis (CH_2Cl_2): λ_{max}/nm = 420, 516, 551, 591, 647.

dx.doi.org/10.1021/ic3016035 | Inorg. Chem. 2012, 51, 10704−10714

7. meso-Mono[o-5-(N-imidazolyl)valeramidophenyl]-triphenylporphyrinatoiron(III) Bromide. This compound was prepared as described above for **3**. Anal. Calcd for $C_{52}H_{39}BrFeN_7O$: C, 68.36; H, 4.30; N, 10.73. Found: C, 67.05; H, 5.10; N, 9.94.

UV−vis (CH_2Cl_2): λ_{max}/nm = 320, 416, 510, 567.

^{1}H NMR ($CDCl_3$): δ −5.32 to −0.83 (−CH_2− proton), 79.11−81.12 (β-pyrrole proton).

*8. meso-Mono(o-5-chlorovaleramidophenyl)-triaminophenylporphyrin (**8**).* To a solution of TAPP[37] (100 mg, 0.148 mmol) taken in 20 mL of dry THF was added dropwise 5-chlorovaleryl chloride (23 μL, 1.2 equiv), and the reaction mixture was stirred for 1 h. To this reaction mixture were added dropwise DCM and aqueous ammonia, and after workup, the organic layer was collected, dried over anhydrous Na_2SO_4, and purified by column chromatography using a 90% DCM/hexane mixture as the eluent. Yield: 82 mg (∼70%).

Anal. Calcd for $C_{64}H_{65}ClN_8O_4$: C, 73.51; H, 6.27; N, 10.72. Found: C, 72.25; H, 6.75; N, 10.35. ESI-MS (positive-ion mode, CH_3CN): m/z 793 (100%; $[M]^+$).

*9. meso-Tris(α,α,α-o-pivalamidophenyl-α-o-5-chlorovaleramidophenyl)porphyrin (**9**).* To the solution of **8** (100 mg, 0.125 mmol) in 20 mL of dry THF, (1.2 equiv × 3) of pyridine was added followed by the dropwise addition of pivolyl chloride (70 μL, 4.5 equiv) and the reaction mixture was stirred for 1 h. DCM and aqueous ammonia were added to this reaction mixture and after workup, the organic layer was collected, dried over anhydrous Na_2SO_4, and purified by column chromatography using a 1% MeOH/DCM mixture as the eluent. Yield: 105 mg (∼80%).

Anal. Calcd for $C_{64}H_{65}ClN_8O_4$: C, 73.51; H, 6.27; N, 10.72. Found: C, 72.25; H, 6.75; N, 10.35. ESI-MS (positive-ion mode, CH_3CN): m/z 1045 (100%; $[M]^+$). ^{1}H NMR ($CDCl_3$): δ −2.62 (s, 2H), 0.06 (s, 6H), 0.25 (s, 18H), 0.4 (s, 3H), 1.87 (m, 4H), 2.8 (m, 4H), 7.1 (m, 2H), 7.47 (m, 6H), 7.93 (m, 8H), 8.71 (m, 4H), 8.84 (s, 8H).

*10. meso-Tris(α,α,α-o-pivalamidophenyl-α-o-5-thioacetatovaleramidophenyl)porphyrin (**10**).* To the solution of **9** (100 mg, 0.095 mmol) taken in 20 mL of dry and degassed acetone, potassium thioacetate (13 mg, 1.2 equiv) was added and the reaction was stirred for 8 h under N_2 atmosphere. After evaporation of the solvent in a rotary evaporator, the reaction was quenched with H_2O, and DCM was added to collect the product in the organic layer. It was dried over anhydrous Na_2SO_4 and purified by column chromatography using a 5% MeOH/DCM mixture. Yield: 72.67 mg (∼70%).

Anal. Calcd for $C_{66}H_{68}N_8O_5S$: C, 73.04; H, 6.31; N, 10.32. Found: C, 72.05; H, 6.80; N, 10.02. ESI-MS (positive-ion mode, MeOH): m/z 1085.37 (100%; $[M]^+$).

*11. meso-Tris(α,α,α-o-pivalamidophenyl-α-o-5-thioacetatovaleramidophenyl)porphyrinatoiron(III) Bromide (**11**).* To the solution of thioacetate-functionalized porphyrin **10** (100 mg, 0.092 mmol) in 15 mL of dry and degassed THF, 2,4,6-collidine was added (25 μL, 2 equiv) followed by the addition of $FeBr_2$ (80 mg, 4 equiv) to this solution. The solution was stirred overnight in a glovebox. The reaction mixture was worked up by H_2O followed by the addition of DCM. The organic layer was washed with a brine solution and collected. It was dried over anhydrous Na_2SO_4 and purified by column chromatography using a 93:7 dry DCM/MeOH mixture in a N_2 atmosphere. Yield: 89 mg (85%).

*12. meso-Tris(α,α,α-o-pivalamidophenyl-α-o-5-thiolvaleramidophenyl)porphyrinatoiron(III) Bromide (**12**).* Thioacetate-functionalized iron porphyrin **11** (100 mg, 0.087 mmol) was dissolved in 15 mL of a degassed mixture of concentrated HCl and MeOH (1:14) and refuxed overnight under N_2 atmosphere in the dark. The reaction mixture was poured into H_2O followed by the addition of DCM. The organic layer was collected and dried over anhydrous Na_2SO_4. It was purified by column chromatography using a 95:5 dry DCM/MeOH mixture in N_2 atmosphere. Yield: 77 mg (80%).

*13. meso-Tris(α,α,α-o-pivalamidophenyl-α-o-5-thiolatevaleramidophenyl)porphyrinatoiron(III) (**13**).* To the solution of thiol-functionalized porphyrin **12** (77 mg, 0.069 mmol) in 15 mL of dry and degassed MeOH, activated K_2CO_3 was added. The solution was stirred overnight in a glovebox. The reaction mixture was filtered, and the filtrate was evaporated and dried by a vacuum pump inside the box. Yield: 70 mg (90%). ESI-MS (positive-ion mode, MeOH): m/z 1093.5742 (100%; $[M]^+$).

Computational Details. All calculations were performed at the IACS computer cluster using *Gaussian 03* software.[53] Both BP86 and B3LYP functionals were used, and a mixed basis set with 6-311g* on the Fe, N, O, and S atoms and 6-31g* on the C and H atoms was used for optimization.[54−57] For the final energy and ground-state calculations, a 6-311+g* basis set on all atoms was used. Frequency calculations were performed using the basis set used for optimization, and no negative frequencies were found for the structures reported. The Mulliken populations were analyzed using *QMforge* software.

RESULTS

A. EPR. The X-band EPR data of the PSR, PIM, and PPSR complexes in weakly coordinating solvents like THF or DCM show an axial HS signal at g = 6 (Figure 3), indicative of a $S = {}^5/_2$ ground state (GS). The EPR data of the precursor thiol complex (PSHR) also shows a HS signal under the same conditions (Figure S-17 in the Supporting Information).[58]

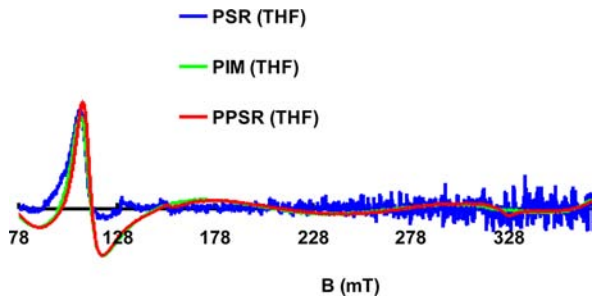

Figure 3. X-band EPR data of the PSR, PIM, and PPSR complexes in THF at 77 K, 10 mW power, and gain 1 × 10^4.

In a coordinating solvent like MeOH, the PIM complex shows an axial EPR signal with rhombic distortion (g = 6.2 and 5.4), suggesting the formation of a MeOH-bound complex (PIM/MeOH) but retaining its $S = {}^5/_2$ GS (Figure 4, green).

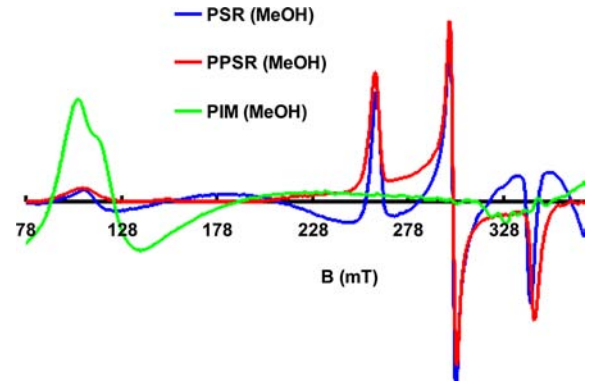

Figure 4. X-band EPR data of the PSR, PPSR, and PIM complexes in MeOH at 77 K, 10 mW power, and gain 1 × 10^4.

Therefore, the PIM complex mimics the coordination and spin-state properties of histidine-coordinated enzyme active sites, e.g., hemoglobin, cytochrome *c* oxidase, etc.; i.e., the 5C and solvent-bound 6C states are both HS. On the contrary, both thiolate-bound complexes, PSR and PPSR, show an $S = {}^1/_2$ GS at 77 K in a coordinating solvent like MeOH (Figure 4, blue

dx.doi.org/10.1021/ic3016035 | *Inorg. Chem.* 2012, 51, 10704−10714

and red). The HS 5C PSR and PPSR complexes are also readily converted to their LS analogue upon the addition of 5−10% MeOH (v/v) to their THF solutions. The g values of the LS PSR and PPSR complexes are similar to those reported for several cyt P450 models and the oxidized resting state of cyt P450 (Table 1).[59] The rhombicity of the LS $S = {}^1/_2$ signal,

Table 1. EPR Parameters for the Heme Thiolate Complexes

	spin	g_1	g_2	g_3	V/λ
cyt P450	${}^1/_2$	2.45	2.26	1.91	4.59
PPSR in MeOH	${}^1/_2$	2.49	2.16	1.90	4.07
PSR in MeOH	${}^1/_2$	2.50	2.16	1.89	3.94

calculated using the Taylor analysis,[60] is similar to those calculated for resting cyt P450 and is consistent with the presence of a strong π-aniosotropic ligand like thiolate.[61] Thus, PSR and PPSR form $S = {}^5/_2$ species in a weakly coordinating solvent and $S = {}^1/_2$ in a coordinating solvent like MeOH. This mimics the GS property of cyt P450, where the 5C substrate-bound state is $S = {}^5/_2$, while the resting 6C H_2O-bound state is $S = {}^1/_2$. Because the linker used to attach the thiolate and imidazole are the same in these complexes, the $S = {}^1/_2$ GS of the 6C MeOH-bound PSR/PPSR complexes relative to the $S = {}^5/_2$ GS of the PIM/MeOH complex must derive from an intrinsic electronic structure difference between these complexes (vide infra).

B. rR. rR is a powerful tool that has been extensively used to diagnose the oxidation state, ligation, and spin state of iron porphyrin complexes.[62] Exciting the intense Soret transition observed in the chromophores yields vibrational information of this macrocycle. Further, the direct coordination of a ligand can be established by observing the corresponding metal−ligand vibration. Only a very few reports of Fe−S vibrations in thiolate-bound iron(III) porphyrin complexes exist in the literature.[63]

The low-temperature (77 K) rR data of the PSR complex in THF show that the oxidation- and spin-state marker ν_4 and ν_2 bands are at 1361 and 1554 cm^{-1} (Figure 5A, red), respectively. The rR data of the PIM complex in DCM show that the ν_4 and ν_2 bands are at 1360 and 1550 cm^{-1} (Figure 5A, black), respectively.[64] However, the rR spectrum of the PSR complex in MeOH shows that the ν_4 and ν_2 bands are at 1369 and 1567 cm^{-1}, respectively (Figure 5A, blue). These values indicate that the Fe center in the PIM and PSR complexes in THF are HS Fe^{III}, while the Fe center in PSR in MeOH is LS Fe^{III}, consistent with the EPR data (Figure 4).[62]

In the low-frequency region, new vibrations are observed for the thiolate-bound $S = {}^1/_2$ PSR/MeOH complex (Figure 5B, blue), at 340, 361, 421, 465, 676, and 770 cm^{-1}, which are not observed for the MeOH-bound PIM complex. This suggests that these vibrations possibly originate because of thiolate coordination to iron(III) porphyrin. The vibrations in the range of 350−470 cm^{-1} may have contribution from the Fe^{III}−S stretching mode (Table 2), while those in the range of 650−800 cm^{-1} may have contribution from the C−S stretching mode.[42,65,63] While confirmed assignment of these vibrations will require isotopic substitution, DFT calculations support these tentative assignments (vide infra). Similarly, the $S = {}^5/_2$ PSR complex in THF shows additional vibrations at 336 and 369 cm^{-1} and at 624, 679, and 765 cm^{-1}. The ν_8 vibrations, which represent the Fe−N_{pyr} (Fe−pyrrole nitrogen) symmetric stretch, are observed at 400 and 391 cm^{-1} for the $S = {}^5/_2$ PIM

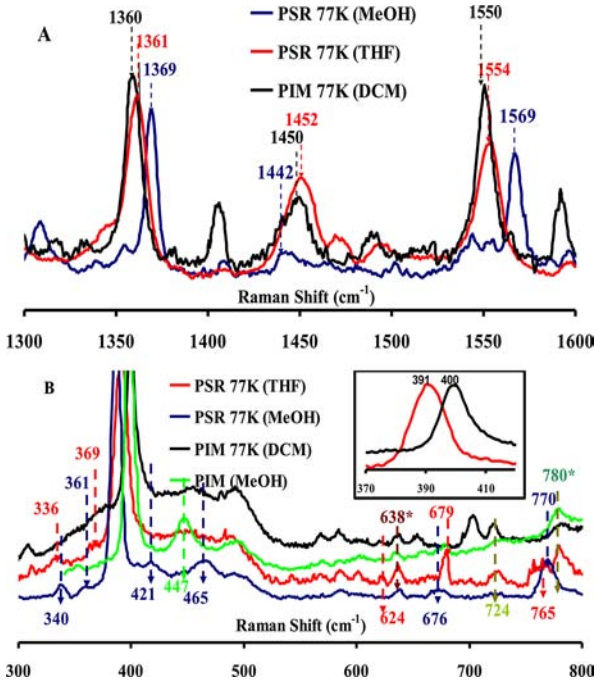

Figure 5. rR data in the (A) high-energy region (1300−1600 cm^{-1}) and rR data in the (B) low-energy region (300−800 cm^{-1}). Laser excitation wavelength = 413.1 nm; power = 10 mW.

Table 2. Selected Fe−S Modes of Synthetic Heme Thiolate Models and Native P450 Complexes

complex	HS/LS	ν_{Fe-S} (cm^{-1})	ref
PSR in THF	HS	369	this work
Higuchi's complex SR	HS	366	42
cyt $P450_{cam}$ (substrate-bound)	HS	350	66, 67
cyt $P450_{BM3}$	HS	356	65, 68
PSR in MeOH	LS	361, 421, 465	this work
Higuchi's complex **1**	LS	394	42

in DCM and the $S = {}^5/_2$ PSR in THF complexes, respectively.[69] The Fe−N_{pyr} vibration reflects the relative donor strengths of the axial ligands between complexes having the same spin states. The data suggest that the $S = {}^5/_2$ PIM complex, which has an axial imidazole ligand, has a stronger Fe−N_{pyr} vibration (400 cm^{-1}) relative to the $S = {}^5/_2$ PSR (391 cm^{-1}) complex, which has a thiolate axial ligand, indicating that the thiolate is a much better donor than imidazole. DFT calculations have been utilized to understand this effect in detail (vide infra).

Note that, in general, Fe−S vibrations have only been observed by using excitation in the UV region (330−360 nm).[42,65] However, here the rR data suggest that the Fe−S vibrations are possibly observed by exciting the Soret band. This implies mixing of the porphyrin and the Fe−S bonding orbitals in these complexes (vide infra).

C. CV. The PSR complex in MeOH shows two oxidation reduction processes (Figure 6, red). The quasi-reversible wave with $E_{1/2}$ of −0.49 V (i.e., −0.3 V vs NHE) represents the $Fe^{III/II}$ couple, consistent with the values reported for the resting cyt P450 (−0.2 V vs NHE) and related LS models.[15,42,70] There is also a one-electron process at −1.09 V, possibly representing the reduction of the porphyrin ring (P) to an anion radical species ($P^{\bullet-}$).[71] In THF solvent, the $Fe^{III/II}$ $E_{1/2}$ of the PSR complex is −0.56 V. The $P/P^{\bullet-}$ process is irreversible in this solvent and is observed around −0.9 V. The

dx.doi.org/10.1021/ic3016035 | Inorg. Chem. 2012, 51, 10704−10714

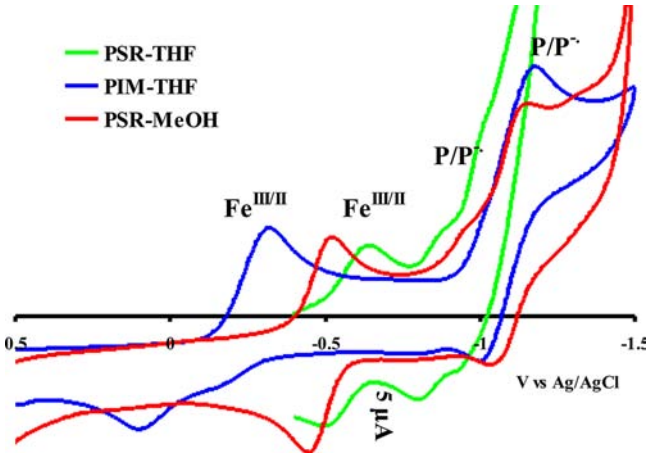

Figure 6. CV of the PSR (red) and PIM (blue) complexes in a MeOH solvent having 100 mM TBAP as the supporting electrolyte, glassy carbon as the working electrode, scan rate = 1 V/s, and Ag/AgCl-saturated KCl as the reference electrode. The individual redox processes are described in the text.

reason for this phenomenon is unclear at this point. The difference between $E_{1/2}$ observed in THF and MeOH have contribution from the spin state (PSR is HS in THF and LS in MeOH from the 77 K EPR data) and hydrogen bonding from the MeOH solvent to the thiolate ligands, which are known to tune reduction potentials up by as much as 300 mV.[43,46] For the PIM complex, in a noncoordinating THF solvent, the $Fe^{III/II}$ couple is observed at −0.13 V and the one-electron P/$P^{\bullet-}$ redox couple is observed at −1.14 V (Figure 6, blue). Thus, the presence of the axial thiolate ligand in PSR lowers the $Fe^{III/II}$ potential by 0.5 V relative to the neutral imidazole ligand in PIM. Note that the ligand framework, spin state, and solvent remain the same between PIM and PSR; this shift in E^0 mainly reflects the effect of substituting a neutral imidazole axial ligand with an anionic axial thiolate ligand.

D. DFT Calculations. *I. Geometry.* Geometry-optimized DFT calculations provide insight into the geometric and electronic structures of these complexes. (Geometry optimizations were performed in *Gaussian 03* using both B3LYP and BP86 functionals.[54−57,73]) The optimized Fe−S bond lengths (Table 3) agree with those reported for HS (2.3−2.4 Å) and LS (2.20−2.25 Å) thiolate-bound heme complexes and active sites,

Table 3. Optimized Bond Lengths (Å) of the Models and Relevant Mulliken[72] Charges

model	method	Fe−N/S	Fe−N_{pyr}	Fe−X_{axial}	q_{Fe}	$q_{N/S}$	q_{pyr}
$S = {}^5/_2$ PIM	BP86	2.08	2.05		1.52	−0.58	−0.74
$S = {}^5/_2$ PIM/MeOH	BP86	2.17	2.08	2.28	1.61	−0.52	−0.71
$S = {}^1/_2$ PIM/MeOH	BP86	1.94	2.00	2.02	1.33	−0.47	−0.66
$S = {}^5/_2$ PSR	B3LYP	2.33	2.08		1.53	−0.49	−0.76
	BP86	2.31	2.09		1.41	−0.41	−0.71
$S = {}^1/_2$ PSR/MeOH	B3LYP	2.23	2.00	2.18	1.28	−0.33	−0.69
	BP86	2.19	2.00	2.15	1.16	−0.25	−0.64

and these values do not vary significantly between functionals.[19,42,44,45,74] The optimized bond lengths of PIM agree reasonably well with the values reported for HS imidazole-bound iron porphyrin complexes.[61] In general, the Fe−N_{pyr} and Fe−L (where L = axial ligand) distances are shorter in the LS complexes. The Fe−N_{pyr} bonds are longer by 0.03 Å in the HS thiolate-bound PSR complex relative to the HS imidazole-bound PIM complex, indicating a weaker Fe−N_{pyr} bond in the former.

ii. Vibrations. The calculated vibrational frequencies (using both BP86 and B3LYP) are listed in Table 4. The calculations indicate that the BP86 functional reproduces (Table 4) the experimentally observed symmetric intraligand modes for the thiolate-bound complexes with good accuracy (within ±10 cm^{-1}). The predicted values for the imidazole linker are lower than the experimental values by 7−30 cm^{-1}. Note that, although the absolute values of the error are large, the percent errors are within ±2−3% of the experimental values. The calculations reproduce the experimentally observed increase in the ν_4 and ν_2 vibrations from 1361 to 1367 cm^{-1} and from 1550 to 1566 cm^{-1} associated with the change of the spin state from HS to LS. These also reproduce the experimentally observed relative magnitudes in the ν_8 vibrations (i.e., the Fe−N_{pyr} stretch) of the HS complexes, i.e., PIM > PIM/MeOH > PSR. Thus, the BP86 functional is used for all other calculations presented in the manuscript.

For the 5C HS PSR model, vibrations at 410, 369, and 308 cm^{-1} have contributions from the Fe−S stretching mode. This suggests that the unique vibration observed at 369 cm^{-1} in the rR spectrum of PSR in THF (experimentally 5C HS) may represent a Fe−S vibration. These values are in the range of Fe−S vibrations reported for cyt P450 and related model complexes that vary between 300 and 360 cm^{-1}.[42,65,66] The C−S stretching mode is calculated to be at 629 cm^{-1}, and indeed there are several weak vibrations observed for the PSR (not PIM) complex in this region. The calculations indicate that vibrations at 446, 414, 375, and 319 cm^{-1} have components of the Fe−S stretching mode in the LS MeOH-bound PSR model. The Fe−S vibrations of LS heme thiolate complexes are reported to be between 360 and 390 cm^{-1}, consistent with the values observed here.[42] The C−S vibration is calculated to be at 637 cm^{-1}. Several vibrations are observed in the rR spectrum of the PSR/MeOH complex only in these regions, consistent with the calculations. Note that while the DFT calculations support these tentative assignments, these assignments can only be confirmed by appropriate isotopic substitution.

iii. Electronic Structure. A. 5C. The GS wave function of the 5C PIM and PSR complexes show a square-pyramidal ligand field (Figure 8), as reported for similar complexes.[19,43,75] The $d_{x^2-y^2}$ orbital is calculated to be highest in energy for both of these models because of its strong interaction with the equatorial N atoms. The imidazole ligand forms a σ bond with the d_{z^2} orbital (Figure 8, left). The d_{z^2} orbital also has its electron density in the *XY* plane, which allows overlap of the porphyrin N atoms with it, as reflected by ∼7% porphyrin N character in the d_{z^2} orbital (Table 5).[43] Note that there is ∼3% mixing between the imidazole N orbitals and the t_2 orbitals on the Fe, i.e., very weak π overlap. Alternatively, the thiolate ligand has a π-bonding interaction with the d_{yz} orbital and a *pseudo*-σ-bonding interaction with the d_{z^2} orbital.[19,43] As a result, the d orbitals with antibonding ligand contributions are at higher energy in PSR relative to these orbitals of the PIM complex (the energies of these orbitals are normalized with

dx.doi.org/10.1021/ic3016035 | *Inorg. Chem.* 2012, 51, 10704−10714

Table 4. Calculated Vibrational Frequencies (cm^{-1})

	PSR			PSR/MeOH			PIM		PIM/MeOH	
mode	rR	BP86	B3LYP	rR	BP86	B3LYP	rR	BP86	rR	BP86
ν_2	**1554**	1551	1604	**1566**	*1563*	1615	**1551**	*1533*	**1550**	*1526*
ν_3	**1451**	1447	1496		*1458*	1508	**1461**	*1427*	**1446**	*1415*
ν_4	**1361**	1351	1395	**1366**	*1359*	1403	**1361**	*1353*	**1361**	*1348*
ν_8	**391**	378	392	**387**	*395*	392	**400**	*383*	**398**	*382*
Fe−S	**336**	308	305	**340**	*319*	319				
	369	369	319	**361**	*375*	359				
		410	369	**421**	*414*	377				
				465	*446*	456				
C−S	**624**	629	640	**673**	*637*	653				
	679									

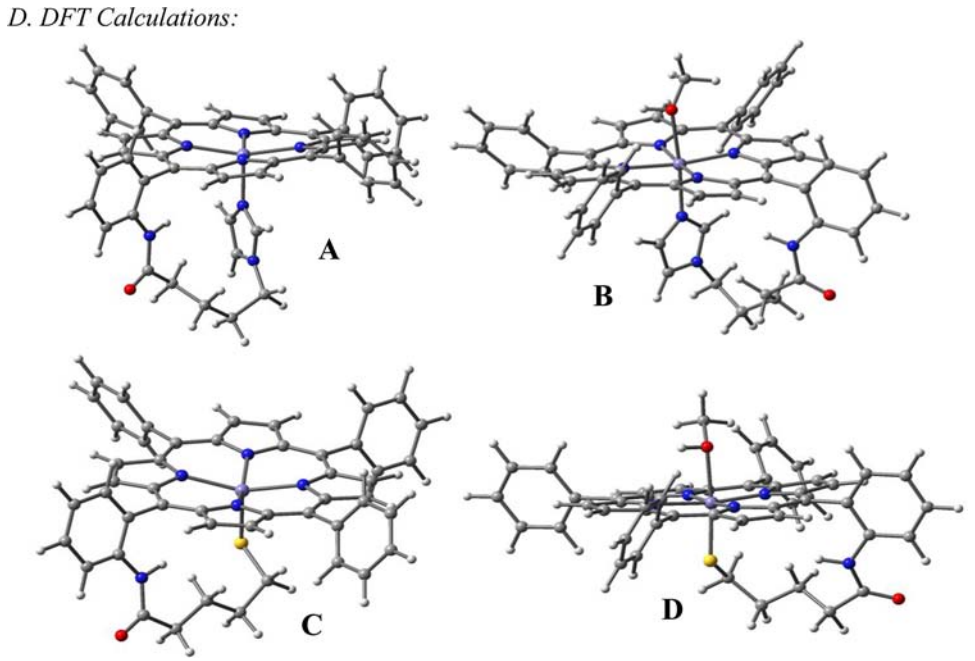

Figure 7. DFT-optimized structures of complexes (A) PIM, (B) PIM/MeOH, (C) PSR, and (D) PSR/MeOH.

respect to the d_{xy} orbital, which is nonbonding in both complexes). The molecular orbital (MO) contributions (Table 5) reveal that the d_{yz} orbital in the PSR model has 28% S_{3p} mixed into it, while the d_{z^2} orbital has 16% S_{3p} mixed into it; i.e., there is significant covalent interaction between Fe and S (both σ and π). On the contrary, the d_{z^2} orbital of the PIM complex has only 7% N contribution. Thus, the Fe−S bond is a lot more covalent than the Fe−imidazole bond. Note that the $d_{x^2-y^2}$ orbital of the PIM complex is at a higher energy than that of the PSR complex. This reflects a weakening of the Fe−N_{pyr} bonds in the PSR complex relative to the PIM complex. The calculated Mulliken charges (q_{Fe}) suggest a lower Z_{eff} on the Fe in the PSR complex due to the covalent donation by the thiolate relative to the Fe in the PIM complex (Table 3; q_{Fe}). The higher Z_{eff} on the Fe in the PIM complex will result in lower-energy unoccupied Fe_{3d} orbitals and allows stronger σ-bonding interaction with the occupied anionic porphyrin donor ligand orbitals (in-plane pyrrole orbitals). The higher Z_{eff} on the Fe will also enhance its electrostatic interaction with the dianionic porphyrin ligand. Overall, these will lead to strong Fe−N_{pyr} bonds in the PIM complex relative to the PSR complex. This is evident from the shorter Fe−N_{pyr} bond lengths and the stronger, i.e., Fe−N_{pyr}, vibrations.

Furthermore, the strong *pseudo-σ*-bonding interaction between the d_{z^2} orbital and the thiolate 3p orbital transfers significant charge density from RS^- to Fe, lowering its Z_{eff}, which raises its energy and allows it to mix with a low-lying π^* orbital of the porphyrin ring (Figure 8, highlighted with a green box). Note that this mixing is also enhanced by the fact that the Fe is ∼0.45 Å above the porphyrin plane in the optimized structure of the PSR complex (Figure 7) relative to 0.3 Å in the optimized structure of the PIM complex (Figure 7). This mixing transfers both Fe d_{z^2} and S_{3p} (because it is involved in σ bonding with the d_{z^2} orbital) character into the porphyrin π^* orbital; i.e., the Fe−S σ^* orbital gains some porphyrin π^* nature and vice versa. This electronic structure may explain the observation of Fe−S and C−S vibrations upon excitation of the porphyrin $\pi \rightarrow \pi^*$ transitions (Soret band).

B. 6C. The GS wave function of the HS 6C PIM/MeOH complex is very similar to that of the PIM complex. It has a distorted octahedral ligand field. Compared to the 5C PIM complex, the d_{z^2} orbital in the 6C PIM/MeOH complex has a slightly elevated energy because of interaction with the MeOH ligand.

The GS wave function of the 6C LS PSR/MeOH complex shows a normal $t_2^5e^0$ electronic structure. The singly occupied

dx.doi.org/10.1021/ic3016035 | *Inorg. Chem.* 2012, 51, 10704−10714

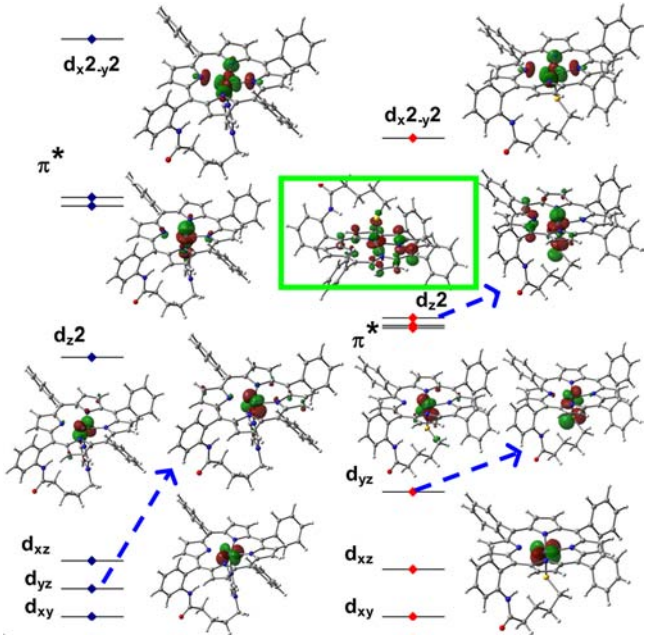

Figure 8. Calculated (BP86) GS MO diagram of 5C PIM (left) and PSR (right) complexes. Only unoccupied β orbitals are shown. The π^* orbital interacting with d_{z^2} is highlighted in the center.

Table 5. MO Compositions of the Unoccupied β Orbitals for the 5C HS Complexes

		orbital contributions		
complex	orbital	Fe_{3d}	L	N_{2p}
PIM	$d_{x^2-y^2}$	66.51	0.00	16.49
	d_{z^2}	66.6	6.69	6.19
	d_{yz}	72.1	0.91	2.89
	d_{xz}	71.22	2.29	3.1
	d_{xy}	85.49	0.08	1.32
PSR	$d_{x^2-y^2}$	68.01	0.00	14.92
	π^*	22.74	6.51	7.17
	d_{z^2}	45.34	15.87	5.84
	d_{yz}	53.48	28.64	1.8
	d_{xz}	70.54	1.03	1.52
	d_{xy}	89.47	0.42	0.42

d_{yz} t_2 orbital forms a π bond (Figure 9, A), while the unoccupied d_{z^2} e orbital forms a σ bond (Figure 9, B) with the thiolate ligand. Because the e set of orbitals are unoccupied (in the HS state, it is half-occupied), both Fe−S and Fe−N_{pyr} σ bonds have a bond order of 1 relative to 0.5 in the HS state. Hence, these bonds are much shorter in the LS state relative to the HS state (Table 3). A noticeable difference in the electronic

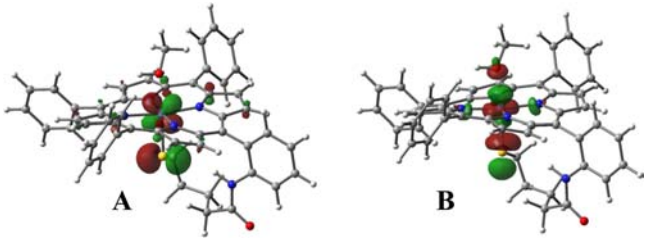

Figure 9. MO overlap (PSR) between (A) d_{yz} and S_{3p} (π bonding) and (B) d_{z^2} and S_{3p} (σ bonding) for the 6C PSR/MeOH complex.

structure of the 6C HS PIM/MeOH and 6C LS PSR/MeOH complexes is the extent of back-bonding from the occupied t_2 orbital to a low-lying unoccupied porphyrin π^* orbital (Figure 10). In the PIM/MeOH complex ~4.8% of the occupied Fe t_2

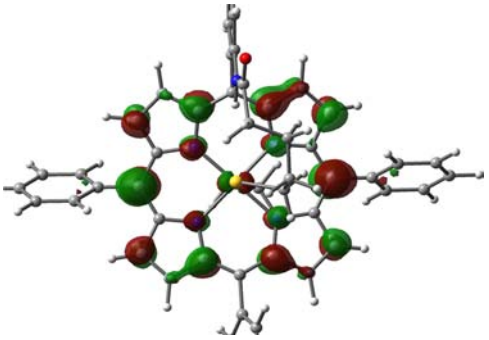

Figure 10. Orbital overlap (PSR) between filled orbitals of Fe (d_{xz}) and the π^* orbital of porphyrin for the 6C PSR/MeOH complex.

character is mixed into this porphyrin π^* orbital, while in the PSR/MeOH complex ~8.2% of the occupied Fe t_2 character is mixed into this porphyrin π^* orbital. This is due to the higher energies of the Fe_{3d} orbital of the PSR/MeOH complex relative to the PIM/MeOH complex because greater covalent charge donation from the anionic thiolate ligand to the Fe in the PSR/MeOH complex (26% π + 2 × 26% σ = ~0.8 e) lowers the Z_{eff} on the Fe and increases the energy of the 3d manifold. This allows better interaction with the t_2 and π^* orbitals. Note that the d_{yz} orbital, which is raised up in energy by strong π-bonding interaction with the thiolate, carries the unpaired electron.

DISCUSSION

One imidazole-bound and two thiolate-bound iron porphyrin complexes are reported. These ligands are covalently attached to the porphyrin macrocycle using the same flexible linker. While several imidazole- and thiolate-bound ferric models are reported in the literature, their comparison is often complicated by differences in their ligand structures. Here, all these complexes have the same linker and vary only in the coordinating headgroup, i.e., thiolate versus imidazole. The results show that a thiolate ligand tunes the reduction potential down by 500 mV, weakens the Fe−N_{pyr} bond of these complexes, and stabilizes a LS state in the 6C form relative to an imidazole ligand.

Geometry-optimized DFT calculations are used to gain insight into the origin of these differences. The calculations reproduce the experimental observations, and the GS wave function indicates that thiolate forms a strong covalent Fe−S bond; i.e., the metal 3d orbitals are strongly mixed with S_{3p} orbitals. This is consistent with previous reports.[43,76] As a result of this interaction, significant electron density is transferred from the thiolate to the Fe. This reduces the Z_{eff} on the Fe, which shifts the Fe 3d manifold up in energy. The increase of the Fe_{3d} orbital energies reduces its interaction with the occupied donor ligand orbitals of porphyrin, i.e., a weaker Fe−N_{pyr} interaction. This manifests itself through longer Fe−N_{pyr} bonds, lower Fe−N_{pyr} vibrations (ν_8), and lower $d_{x^2-y^2}$ orbital energies for the PSR complex relative to the PIM complex. The increase of the Fe_{3d} orbital energies in the PSR complex facilitate its oxidation (i.e., removal of an electron from the HOMO), consistent with the experimentally observed lowering of the $Fe^{III/II}$ reduction potential relative to the PIM complex.

dx.doi.org/10.1021/ic3016035 | Inorg. Chem. 2012, 51, 10704−10714

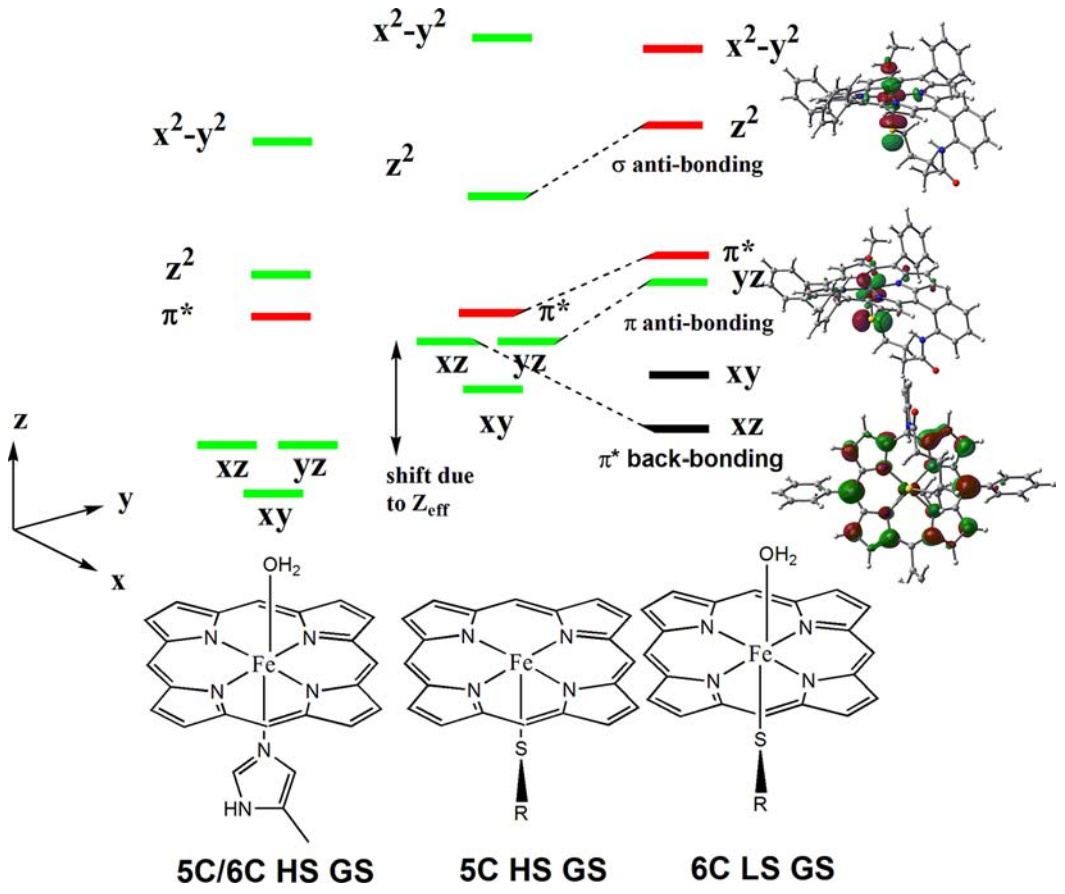

Figure 11. MO interaction between filled orbitals of metal (t_2) with empty orbitals of porphyrin (π^*) and S_{3p} orbital. The green lines represent the singly occupied 3d orbitals, the red lines represent the unoccupied 3d and π^* orbitals, and the black lines represent the occupied 3d orbitals.

Another interesting consequence of thiolate coordination is stabilization of a LS GS in the PSR/MeOH complex in contrast to a HS GS observed in the imidazole-coordinated PIM/MeOH complex. The same spin states are observed in the heme active sites; histidine-bound 6C sites with a trans H_2O ligand are HS, while cysteine-bound 6C sites with a trans H_2O ligand are LS. Considering the fact that a thiolate is a weak-field ligand (i.e., it acts as both σ and π donors), the LS state of a 6C axial thiolate-bound iron(III) porphyrin is rather unexpected. In fact, the 6C axial thiolate-bound nonheme active site of SOR and its synthetic model complexes have a HS GS.[48] The Fe−S bond of this active site is quite covalent, and its covalency is comparable to the covalency of the Fe−S bond of cyt P450 in its resting HS state.[31] The MO diagram of the 6C PSR/MeOH complex reveals that charge transfer from thiolate to Fe^{III} raises the energy of the Fe_{3d} manifold due to lowering of the Z_{eff} of the Fe. This allows back-bonding interaction between the occupied t_2 orbitals on the Fe and the low-lying unoccupied porphyrin π^* orbitals. The extent of back-bonding (measured by the amount of occupied t_2 character mixed into the unoccupied ligand π^* orbitals) is calculated to be 1.8 times more in a 6C LS PSR/MeOH model relative to a 6C LS PIM/MeOH complex. This back-bonding interaction stabilizes the t_2 orbitals involved (d_{xz} and d_{yz}) and thus stabilizes the LS GS state in a thiolate-bound PSR/MeOH complex. The relative position of these porphyrin π^* orbitals will definitely vary depending on the nature of the substitution on the peripheral C atoms. Thus, the extent of back-bonding, i.e., the extent of stabilization of the LS GS, may vary depending on the nature of the porphyrin ligand. Note that the back-bonding is not observed in the HS complexes because (1) the t_2 orbitals are half-occupied and (2) the covalent charge transfer is much more in the LS state because the Fe−S bond lengths are shorter and the e orbitals are completely unoccupied in the LS state and not half-occupied as in the HS state.

Thus, the thiolate ligand tunes the electronic structure of a HS iron(III) poprphyrin via direct orbital interactions (Figure 11), where it raises the energy of the d_{z^2} and one of the t_2 orbitals (d_{yz} in the nomenclature used here) because of *pseudo*-σ- and π-bonding interactions, respectively. The covalent charge donation from the anionic thiolate ligand also raises the energy of the 3d manifold in general (Figure 11, middle) relative to that of a neutral imidazole ligand. This increase of the Fe_{3d} manifold affects bonding interactions of the Fe_{3d} orbitals that the thiolate does not have any direct overlap with it. The increase in energy of the d_{xy} orbital (the redox-active orbital in the HS complexes) lowers E^0 of these HS complexes (as observed experimentally), and the increase in energy of the $d_{x^2-y^2}$ orbital weakens its interaction with the occupied lower-energy porphyrin pyrrole orbitals weakening the Fe−N_{pyr} bond (longer Fe−N bonds in optimized structure and lower ν_8 vibration) of the HS complexes. Further, the increase in energy of the noninteracting t_2 orbital along the Fe−S bond (d_{xz} in the nomenclature used here) increases its back-bonding interaction with a low-lying porphyrin π^* orbital (Figure 11, right) and lowers its energy. As a result of destabilization of the d_{z^2} orbital due to *pseudo*-σ-bonding interaction with thiolate and the trans axial MeOH ligand and

dx.doi.org/10.1021/ic3016035 | *Inorg. Chem.* 2012, 51, 10704−10714

stabilization of the d_{xz} orbital due to back-bonding, the 6C thiolate-bound PSR/MeOH complex stabilizes a LS GS; an electronic structure contribution possibly is present in many thiolate-bound porphyrin active sites and synthetic complexes.

■ ASSOCIATED CONTENT

Supporting Information

Characterization of the complexes, EPR data of thiol complexes, rR data of thiol complexes, and optimized geometries. This material is available free of charge via the Internet at http://pubs.acs.org.

■ AUTHOR INFORMATION

Corresponding Author

*E-mail: icad@iacs.res.in.

Notes

The authors declare no competing financial interest.

■ ACKNOWLEDGMENTS

This work is funded by Council of Scientific and Industrial Research (CSIR), India [Grant 01(2412)10/EMr-II], and the Department of Science and Technology, India (Grant SR/IC-35/2009). P.K.D. and S.C. acknowledge a CSIR JRF fellowship. S.S. acknowledges the IACS integrated Ph.D. program.

■ REFERENCES

(1) Green, M. T. *Curr. Opin. Chem. Biol.* **2009**, *13*, 84−88.
(2) Meunier, B.; de Visser, S. P.; Shaik, S. *Chem. Rev.* **2004**, *104*, 3947−3980.
(3) Averill, B. A. *Chem. Rev.* **1996**, *96*, 2951−2964.
(4) Green, M. T.; Dawson, J. H.; Gray, H. B. *Science* **2004**, *304*, 1653−1656.
(5) Shaik, S.; Cohen, S.; Wang, Y.; Chen, H.; Kumar, D.; Thiel, W. *Chem. Rev.* **2012**, *110*, 949−1017.
(6) Riplinger, C.; Neese, F. *ChemPhysChem* **2011**, *12*, 3192−3203.
(7) Ogliaro, F.; Cohen, S.; Filatov, M.; Harris, N.; Shaik, S. *Angew. Chem., Int. Ed.* **2000**, *39*, 3851−3855.
(8) Rittle, J.; Green, M. T. *Science* **2010**, *330*, 933−937.
(9) Cramer, S. P.; Dawson, J. H.; Hodgson, K. O.; Hager, L. P. *J. Am. Chem. Soc.* **1978**, *100*, 7282−7290.
(10) Dawson, J. H. *Science* **1988**, *240*, 433−439.
(11) Ogliaro, F.; Cohen, S.; de Visser, S. P.; Shaik, S. *J. Am. Chem. Soc.* **2000**, *122*, 12892−12893.
(12) Altun, A.; Kumar, D.; Neese, F.; Thiel, W. *J. Phys. Chem. A* **2008**, *112*, 12904−12910.
(13) Green, M. T. *J. Am. Chem. Soc.* **1998**, *120*, 10772−10773.
(14) Shaik, S.; Kumar, D.; de Visser, S. P. *J. Am. Chem. Soc.* **2008**, *130*, 10128−10140.
(15) Sligar, S. G. *Biochemistry* **1976**, *15*, 5399−5406.
(16) Newcomb, M.; Zhang, R.; Chandrasena, R. E. P.; Halgrimson, J. A.; Horner, J. H.; Makris, T. M.; Sligar, S. G. *J. Am. Chem. Soc.* **2006**, *128*, 4580−4581.
(17) Ogliaro, F.; de Visser, S. P.; Shaik, S. *J. Inorg. Biochem.* **2002**, *91*, 554−567.
(18) Shaik, S.; Kumar, D.; de Visser, S. P.; Altun, A.; Thiel, W. *Chem. Rev.* **2005**, *105*, 2279−2328.
(19) Green, M. T. *J. Am. Chem. Soc.* **1999**, *121*, 7939−7940.
(20) Dawson, J. H.; Sono, M. *Chem. Rev.* **1987**, *87*, 1255−1276.
(21) Sono, M.; Andersson, L. A.; Dawson, J. H. *J. Biol. Chem.* **1982**, *257*, 8308−8320.
(22) Sligar, S. G. *Science* **2010**, *330*, 924−925.
(23) Schlichting, I.; Berendzen, J.; Chu, K.; Stock, A. M.; Maves, S. A.; Benson, D. E.; Sweet, R. M.; Ringe, D.; Petsko, G. A.; Sligar, S. G. *Science* **2000**, *287*, 1615−1622.
(24) Schoeneboom, J. C.; Neese, F.; Thiel, W. *J. Am. Chem. Soc.* **2005**, *127*, 5840−5853.
(25) Rittle, J.; Younker, J. M.; Green, M. T. *Inorg. Chem.* **2010**, *49*, 3610−3617.
(26) Kumar, D.; Sastry, G. N.; de Visser, S. P. *Chem.—Eur. J.* **2011**, *17*, 6196−6205.
(27) de Visser, S. P.; Latifi, R.; Tahsini, L.; Nam, W.-W. *Chem.—Asian J.* **2011**, *6*, 493−504.
(28) Kumar, D.; Karamzadeh, B.; Sastry, G. N.; de Visser, S. P. *J. Am. Chem. Soc.* **2010**, *132*, 7656−7667.
(29) de Visser, S. P.; Tahsini, L.; Nam, W. *Chem.—Eur. J.* **2009**, *15*, 5577−5587.
(30) de Visser, S. P. *Biochem. Soc. Trans.* **2009**, *37*, 373−377.
(31) Dey, A.; Jiang, Y.; Ortiz de Montellano, P.; Hodgson, K. O.; Hedman, B.; Solomon, E. I. *J. Am. Chem. Soc.* **2009**, *131*, 7869−7878.
(32) Kumar, D.; Sastry, G. N.; de Visser, S. P. *J. Phys. Chem. B* **2012**, *116*, 718−730.
(33) Deng, T. j.; Macdonald, I. D. G.; Simianu, M. C.; Sykora, M.; Kincaid, J. R.; Sligar, S. G. *J. Am. Chem. Soc.* **2001**, *123*, 269−278.
(34) Usharani, D.; Zazza, C.; Lai, W.; Chourasia, M.; Waskell, L.; Shaik, S. *J. Am. Chem. Soc.* **2012**, *134*, 4053−4056.
(35) Chang, C. K.; Dolphin, D. *J. Am. Chem. Soc.* **1975**, *97*, 5948−5950.
(36) Chang, C. K.; Dolphin, D. *J. Am. Chem. Soc.* **1976**, *98*, 1607−1609.
(37) Collman, J. P.; Gagne, R. R.; Reed, C.; Halbert, T. R.; Lang, G.; Robinson, W. T. *J. Am. Chem. Soc.* **1975**, *97*, 1427−1439.
(38) Collman, J. P.; Sorrell, T. N. *J. Am. Chem. Soc.* **1975**, *97*, 4133−4134.
(39) Traylor, T. G.; Mincey, T. C.; Berzinis, A. P. *J. Am. Chem. Soc.* **1981**, *103*, 7084−7089.
(40) Traylor, T. G.; Nolan, K. B.; Hildreth, R. *J. Am. Chem. Soc.* **1983**, *105*, 6149−6151.
(41) Tani, F.; Matsu-ura, M.; Nakayama, S.; Naruta, Y. *Coord. Chem. Rev.* **2002**, *226*, 219−226.
(42) Suzuki, N.; Higuchi, T.; Urano, Y.; Kikuchi, K.; Uekusa, H.; Ohashi, Y.; Uchida, T.; Kitagawa, T.; Nagano, T. *J. Am. Chem. Soc.* **1999**, *121*, 11571−11572.
(43) Dey, A.; Okamura, T.; Ueyama, N.; Hedman, B.; Hodgson, K. O.; Solomon, E. I. *J. Am. Chem. Soc.* **2005**, *127*, 12046−12053.
(44) Ueyama, N.; Nishikawa, N.; Yamada, Y.; Okamura, T.; Nakamura, A. *J. Am. Chem. Soc.* **1996**, *118*, 12826−12827.
(45) Higuchi, T.; Uzu, S.; Hirobe, M. *J. Am. Chem. Soc.* **1990**, *112*, 7051−7053.
(46) Ueyama, N.; Nishikawa, N.; Yamada, Y.; Okamura, T.-a.; Oka, S.; Sakurai, H.; Nakamura, A. *Inorg. Chem.* **1998**, *37*, 2415−2421.
(47) Collman, J. P.; Boulatov, R.; Sunderland, C. J.; Fu, L. *Chem. Rev.* **2003**, *104*, 561−588.
(48) Dey, A.; Jenney, F. E.; Adams, M. W. W.; Johnson, M. K.; Hodgson, K. O.; Hedman, B.; Solomon, E. I. *J. Am. Chem. Soc.* **2007**, *129*, 12418−12431.
(49) Clay, M. D.; Jenney, F. E.; Hagedoorn, P. L.; George, G. N.; Adams, M. W. W.; Johnson, M. K. *J. Am. Chem. Soc.* **2001**, *124*, 788−805.
(50) Collman, J. P.; Brauman, J. I.; Doxsee, K. M.; Halbert, T. R.; Bunnenberg, E.; Linder, R. E.; LaMar, G. N.; Del Gaudio, J.; Lang, G.; Spartalian, K. *J. Am. Chem. Soc.* **1980**, *102*, 4182−4192.
(51) Mashiko, T.; Reed, C. A.; Haller, K. J.; Kastner, M. E.; Scheidt, W. R. *J. Am. Chem. Soc.* **1981**, *103*, 5758−5767.
(52) Berto, T. C.; Praneeth, V. K. K.; Goodrich, L. E.; Lehnert, N. *J. Am. Chem. Soc.* **2009**, *131*, 17116−17126.
(53) Frisch, M. J. T.; et al. *Gaussian 03*, version C.02; Gaussian, Inc.: Wallingford, CT, 2004.
(54) Becke, A. D. *Phys. Rev. A* **1988**, *38*, 3098−3100.
(55) Becke, A. D. *J. Chem. Phys.* **1993**, *98*, 5648−5652.
(56) Perdew, J. P.; Burke, K.; Ernzerhof, M. *Phys. Rev. Lett.* **1996**, *77*, 3865−3868.
(57) Perdew, J. P. *Phys. Rev. B (Condens. Matter)* **1986**, *33*, 8822−8824.
(58) Note that previously a PIM complex with a ClO_4^- counterion was proposed to exist as a mixture of the monomeric complex and a

bis(imidazole) dimer (where an imidazole arm of one monomer binds an Fe of another) in equilibrium. This was supported by the observation of both $S = {}^5/_2$ and ${}^1/_2$ signals in the EPR data of the PIM complex. Here, when a bromide counterion is present, no $S = {}^1/_2$ signal is observed.

(59) Walker, F. A. *Coord. Chem. Rev.* **1999**, *185*−*186*, 471−534.

(60) Taylor, C. P. S. *Biochim. Biophys. Acta, Protein Struct.* **1977**, *491*, 137−148.

(61) Ann, W. F. *Coord. Chem. Rev.* **1999**, *185*−*186*, 471−534.

(62) Burke, J. M.; Kincaid, J. R.; Peters, S.; Gagne, R. R.; Collman, J. P.; Spiro, T. G. *J. Am. Chem. Soc.* **1978**, *100*, 6083−6088.

(63) Kitagawa, T.; Dey, A.; Lugo-Mas, P.; Benedict, J. B.; Kaminsky, W.; Solomon, E.; Kovacs, J. A. *J. Am. Chem. Soc.* **2006**, *128*, 14448−14449.

(64) Note that, as indicated by the EPR data, no LS component is observed in the rR data of PIM in THF/DCM/MeOH. This further diminishes the possibility of the previously reported equilibrium in solution. This could reflect the role of the bromide counterion that is bound to the PIM complex.

(65) Deng, T.; Proniewicz, L. M.; Kincaid, J. R.; Yeom, H.; Macdonald, I. D. G.; Sligar, S. G. *Biochemistry* **1999**, *38*, 13699−13706.

(66) Champion, P. M.; Stallard, B. R.; Wagner, G. C.; Gunsalus, I. C. *J. Am. Chem. Soc.* **1982**, *104*, 5469−5472.

(67) Wells, A. V.; Li, P.; Champion, P. M.; Martinis, S. A.; Sligar, S. G. *Biochemistry* **1992**, *31*, 4384−4393.

(68) Chen, Z.; Ost, T. W. B.; Schelvis, J. P. M. *Biochemistry* **2004**, *43*, 1798−1808.

(69) Paulat, F.; Praneeth, V. K. K.; Nather, C.; Lehnert, N. *Inorg. Chem.* **2006**, *45*, 2835−2856.

(70) Fisher, M. T.; Sligar, S. G. *J. Am. Chem. Soc.* **1985**, *107*, 5018−5019.

(71) Lin, C.; Fang, M. Y.; Cheng, S. H. *J. Electroanal. Chem.* **2002**, *531*, 155−162.

(72) Mulliken, R. S. *J. Chem. Phys.* **1955**, *23*, 1833−1840.

(73) Baerends, E. J.; Ellis, D. E.; Ros, P. *Chem. Phys.* **1973**, *2*, 41−51.

(74) Denisov, I. G.; Makris, T. M.; Sligar, S. G.; Schlichting, I. *Chem. Rev.* **2005**, *105*, 2253−2278.

(75) Note that while both occupied α and unoccupied β orbitals carry the same information; the contours of the unoccupied β orbitals are cleaner. The occupied α orbitals mix with several other occupied ligand-based orbitals that have similar energies

(76) Paulat, F.; Lehnert, N. *Inorg. Chem.* **2007**, *46*, 1547−1549.